AIAA JOURNAL
Vol. 32, No. 7, July 1994

Thermomechanical Buckling of Multilayered Composite Panels with Cutouts

Ahmed K. Noor,* James H. Starnes Jr.,† and Jeanne M. Peters‡
NASA Langley Research Center, Hampton, Virginia 23681

A study is made of the thermomechanical buckling of flat unstiffened composite panels with central circular cutouts. The panels are subjected to combined temperature changes and applied edge loading (or edge displacements). The analysis is based on a first-order shear deformation plate theory. A mixed formulation is used with the fundamental unknowns consisting of the generalized displacements and the stress resultants of the plate. Both the stability boundary and the sensitivity coefficients are evaluated. The sensitivity coefficients measure the sensitivity of the buckling response to variations in the different lamination and material parameters of the panel. Numerical results are presented showing the effects of the variations in the hole diameter, laminate stacking sequence, fiber orientation, and aspect ratio of the panel on the thermomechanical buckling response and its sensitivity coefficients.

Nomenclature

$[A], [B], [D], [A_s]$ = matrices of the extensional, coupling, bending, and transverse shear stiffnesses of the panel
d = diameter of the circular cutout
E_L, E_T = elastic moduli of the individual layers in the direction of fibers and normal to it, respectively
$[F]$ = linear flexibility matrix of the panel, see Eqs. (B2)
G_{LT}, G_{TT} = shear moduli of the individual layers in the plane of fibers and normal to it, respectively
$\{\bar{G}(Z)\}$ = vector of nonlinear terms of the panel, see Eqs. (1)
$\{H\}$ = vector of stress-resultant parameters
h = total thickness of the panel
$[\bar{K}]$ = global linear structural matrix, see Eqs. (1)
$[\bar{K}_1], [\bar{K}_2]$ = geometric stiffness matrices of the panel, see Eqs. (3)
L_1, L_2 = side lengths of the panel in the x_1 and x_2 coordinate directions, respectively
M_1, M_2, M_{12}, M_{21} = bending stress resultants
$\{\bar{M}(X, \bar{X}_e)\}$, $\{\bar{N}(H, X, \bar{X}_e)\}$ = subvectors of nonlinear terms, see Eqs. (B3)
$\bar{N}_1$ = applied compressive edge loading
$\bar{N}_{1,cr}$ = critical value of $\bar{N}_1$
N_1, N_2, N_{12}, N_{21} = in-plane (extensional) stress resultants
NL = number of layers in the panel
$\{N\}, \{M\}$ = vectors of in-plane and bending stress resultants, see Eqs. (A1)
$\{N_T\}, \{M_T\}$ = vectors of thermal forces and moments in the panel, see Eqs. (A1)
$N_{i'}, N_{j'}$ = shape functions used in approximating each of the stress resultants
$\{P\}$ = vector of normalized applied edge loading
Q_1, Q_2 = transverse shear stress resultants
$\{Q\}$ = vector of transverse shear stress resultants
$\{\bar{Q}^{(1)}\}, \{\bar{Q}^{(2)}\}$ = vectors of normalized thermal strains and mechanical loads (or strains)
$[\bar{Q}^{(k)}], [\bar{Q}_s]^{(k)}$ = matrices of the extensional and transverse shear stiffnesses of the kth layer of the plate (referred to x_1, x_2, x_3 coordinate system)
q_e = applied edge displacement
$q_{e,cr}$ = critical value of q_e
q_1, q_2 = thermal strain and edge loading (or edge displacement) parameters associated with $\{\bar{Q}^{(1)}\}$ and $\{\bar{Q}^{(2)}\}$, respectively
$\hat{q}_1, \hat{q}_2$ = critical combination of q_1 and q_2, respectively
$[S_1], [S_2]$ = linear strain-displacement matrices associated with the free nodal displacements $\{X\}$ and the constrained (prescribed nonzero) edge displacements, $q_2\{\bar{X}_e\}$
T_{cr} = critical value of T_0
T_0 = uniform temperature change
U = strain energy density (energy per unit surface area) of the panel
u_1, u_2, w = displacement components in the coordinate directions, see Fig. 1
$\{X\}$ = vector of free (unknown) nodal displacements
$\{\bar{X}_e\}$ = normalized vector of constrained (prescribed nonzero) edge displacements
x_1, x_2, x_3 = Cartesian coordinate system (x_3 normal to the middle plane of the panel)
$\{Z\}$ = response vector of the panel
α_L, α_T = coefficients of thermal expansion of the individual layers in the direction of fibers and normal to it, respectively
$\{\alpha\}^{(k)}$ = vector of coefficients of thermal expansion of the kth layer of the panel (referred to the x_1, x_2, x_3 coordinate system)
$\{\gamma\}$ = vector of transverse shear strain components of the panel, see Eqs. (A1)
$\gamma_{3\beta}$ = transverse shear strains in the panel, $\beta = 1, 2$
$\{\varepsilon\}$ = vector of extensional strain components of the panel, see Eqs. (A1)
$\{\varepsilon_T\}$ = thermal strain subvector, see Eqs. (B4) and Eqs. (C4)
θ = fiber orientation angles of the individual layers
$\{\kappa\}$ = vector of bending strain components of the panel, see Eqs. (A1)
λ_ℓ = lamination and material parameters of the panel

Received Jan. 4, 1993; revision received Sept. 29, 1993; accepted for publication Dec. 7, 1993.

*Ferman W. Perry Professor of Aerospace Structures and Applied Mechanics, and Director, Center for Computational Structures Technology, University of Virginia. Fellow AIAA.
†Head, Aircraft Structures Branch. Fellow AIAA.
‡Senior Programmer Analyst, Center for Computational Structures Technology, University of Virginia.

ν_{LT} = major Poisson's ratio of the individual layers
ϕ_1, ϕ_2 = rotation components of the middle plane of the panel

Subscripts

I' = 1 to the total number of stress-resultant parameters in the model (components of the vector $\{H\}$)
I, J = 1 to the total number of free nodal displacement components in the model (components of the vector $\{X\}$)
i, j = 1 to the total number of degrees of freedom (free nodal displacements and stress resultant parameters) in the model
i', j' = 1 to the total number of shape functions used in approximating each of the stress resultants (within individual elements)
L = direction of fibers
ℓ = 1 to the total number of material and lamination parameters considered
T = transverse direction
T = thermal
β = 1, 2

Superscripts

k = layer
r = iteration cycle
t = matrix transposition

Introduction

CONSIDERABLE literature has been devoted to the study of buckling of isotropic panels with cutouts. More recently, a number of studies considered the buckling of composite panels with cutouts. These included both experimental investigations as well as approximate and numerical studies (see, for example, Refs. 1–10). Except for Refs. 5 and 7, all of the cited references considered only mechanical loading. Because of the increasing use of fibrous composite materials in flight vehicle structures subjected to elevated temperatures, an understanding of the thermomechanical buckling response of composite panels with cutouts is desirable. Moreover, a study of the sensitivity of the buckling response to variations in the material and lamination parameters of these panels is needed to provide an indication of the effects of changes in these parameters on the panel response.

The present study focuses on understanding the detailed buckling response characteristics of multilayered composite panels with cutouts, subjected to combined mechanical and thermal loads, and the sensitivity of these response characteristics to variations in lamination and geometric parameters. The unstiffened flat panels, with central circular holes, considered in the study consist of a number of perfectly bonded layers and are symmetrically laminated with respect to the middle plane. The individual layers are assumed to be homogeneous and anisotropic. A plane of thermoelastic symmetry exists at each point of the panel parallel to the middle plane. The loading consists of a combination of a uniform temperature change and either an applied edge loading or an applied edge displacement. The material properties are assumed to be independent of temperature.

Mathematical Formulation

Governing Finite Element Equations

The analytical formulation is based on a first-order shear deformation, von Kármán-type plate theory with the effects of large displacements, average transverse shear deformation through the thickness, and laminated anisotropic material behavior included. A linear, Duhamel-Neumann type, constitutive model is used, and the material properties are assumed to be independent of temperature. The thermoelastic constitutive relations used in the present study are given in Appendix A. The panel is discretized by using two-field mixed finite element models. The stress resultants are allowed to be discontinuous at interelement boundaries in the model. The sign convention for generalized displacements and stress resultants for the model is shown in Fig. 1. The external loading consists of an applied edge loading $\bar{N}_1$ (or an applied edge displacement q_e) and a uniform temperature change T_0 that is independent of the coordinates x_1, x_2, and x_3.

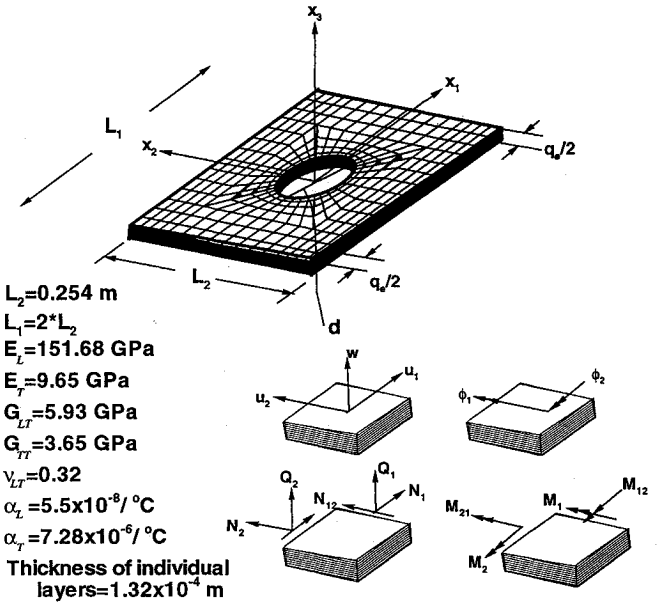

Fig. 1 Panels considered in the present study and sign convention for stress resultants and generalized displacements.

Table 1 Boundary conditions used in the present study

Type[a]	At $x_1 = \pm L_1/2$	At $x_2 = \pm L_2/2$
1d and 1L	$u_2 = w = \phi_2 = 0$	$w = \phi_1 = 0$
2d and 2L	$u_2 = w = \phi_1 = \phi_2 = 0$	$w = \phi_1 = 0$
3d and 3L	$u_2 = w = \phi_1 = \phi_2 = 0$	$u_2 = w = \phi_1 = 0$

[a]d in the boundary condition type refers to prescribed edge displacements $u_1 = \mp q_e/2$, and L refers to prescribed edge loading $\bar{N}_1$ (u_1 is not prescribed).

Table 2 Composite panels considered in the numerical studies[a]

Panels	Panel no.	Laminate stacking sequence
Quasi-isotropic	Q1	$[\pm 45/0/90]_{ns}$
	Q2	$[\pm 45/0/-45/90]_{ns}$
	Q3	$[\pm 45/90/-45/0]_{ns}$
Anisotropic	A1	$[\pm 45]_{2ns}$
	A2	$[\pm 45/90_2]_{ns}$
	A3	$[+45/90/-45/90]_{ns}$
	A4	$[\pm 45/0_2]_{ns}$
	A5	$[+45/0/-45/0]_{ns}$
Cross-ply	C1	$[0/90]_{2ns}$
	C2	$[90/0]_{2ns}$

[a]n = 1, 2, or 3 corresponds to the total number of layers NL = 8, 16, or 24, respectively.

The governing finite element equations describing the nonlinear response of the panel can be written in the following compact form:

$$\{f(Z)\} = [\bar{K}]\{Z\} + \{\bar{G}(Z)\} - q_1\{\bar{Q}^{(1)}\} - q_2\{\bar{Q}^{(2)}\} \quad (1)$$

where $[\bar{K}]$ includes the flexibility and the linear strain-displacement matrices, and $\{Z\}$ includes both unknown (free) nodal displacements and stress-resultant parameters. The form of the arrays $[\bar{K}]$, $\{\bar{G}(Z)\}$, $\{\bar{Q}^{(1)}\}$, and $\{\bar{Q}^{(2)}\}$ is described in Ref. 11 and is given in Appendix B.

Prebuckling State

The prebuckling responses (generalized displacements and stress resultants) associated with the thermal strain and applied

edge loading (or edge displacements), respectively, are given by the following set of linear equations with two right-hand sides (one corresponding to $q_1 = 1$ and $q_2 = 0$, and the other to $q_1 = 0$ and $q_2 = 1$):

$$[\bar{K}]\,[\{Z_1\}\{Z_2\}] = [\{\bar{Q}^{(1)}\}\{\bar{Q}^{(2)}\}] \tag{2}$$

where subscripts 1 and 2 refer to the response vectors associated with the thermal loading and the applied edge loading (or edge displacement), respectively.

Identification and Determination of Stability Boundary

For certain combinations of the two parameters q_1 and q_2, an instability (or bifurcation) occurs. The totality of the critical (or bifurcation) points in the q_1–q_2 space constitutes the stability boundary that separates regions of stability and instability.

If prebuckling deformations are neglected, the equations that determine the stability boundary for the panel can be cast into the form of a linear algebraic eigenvalue problem as follows:

$$([\bar{K}] + \hat{q}_1[\bar{K}_1] + \hat{q}_2[\bar{K}_2])\{\hat{Z}\} = 0 \tag{3}$$

where $\{\hat{Z}\}$ is the associated modal response vector. The explicit forms of $[\bar{K}_1]$ and $[\bar{K}_2]$ are given in Appendix B.

Sensitivity of Buckling Response to Variations in Lamination and Material Parameters

Sensitivity coefficients can be used to study the sensitivity of the thermomechanical buckling response to variations in the different material and lamination parameters of the plate. The expression for the sensitivity coefficients of the critical combination of load parameters with respect to the lamination and material parameters of a composite plate is given by

$$\frac{\partial \hat{q}_1}{\partial \lambda_\ell}\{\hat{Z}\}^t[\bar{K}_1]\{\hat{Z}\} + \frac{\partial \hat{q}_2}{\partial \lambda_\ell}\{\hat{Z}\}^t[\bar{K}_2]\{\hat{Z}\}$$

$$= -\{\hat{Z}\}^t[\bar{K}]\{\hat{Z}\} - \{\hat{Z}\}^t\left[\hat{q}_1\left[\frac{[\partial \bar{K}_2]}{\partial \lambda_\ell}\right] + \hat{q}_2\left[\frac{[\partial \bar{K}_2]}{\partial \lambda_\ell}\right]\right]\{\hat{Z}\} \tag{4}$$

Application of Multiple-Parameter Reduction Method

To reduce the cost of determining the stability boundary for different composite plates, multiple-parameter reduction methods have been developed for substantially reducing the number of degrees of freedom used in the initial discretization. These methods are based on successive applications of the finite element method and the classical Rayleigh-Ritz technique. The finite element method is used to generate a few global approximation vectors (or

Buckling Response

All of the panels considered have symmetric lamination with respect to the middle plane and are assumed to remain flat until buckling. The prebuckling displacements exhibited inversion symmetry characterized by the following relations:

$$\begin{aligned} u_\beta(x_1, x_2) &= -u_\beta(-x_1, -x_2) \\ w(x_1, x_2) &= 0 \\ \phi_\beta(x_1, x_2) &= 0 \end{aligned} \tag{5}$$

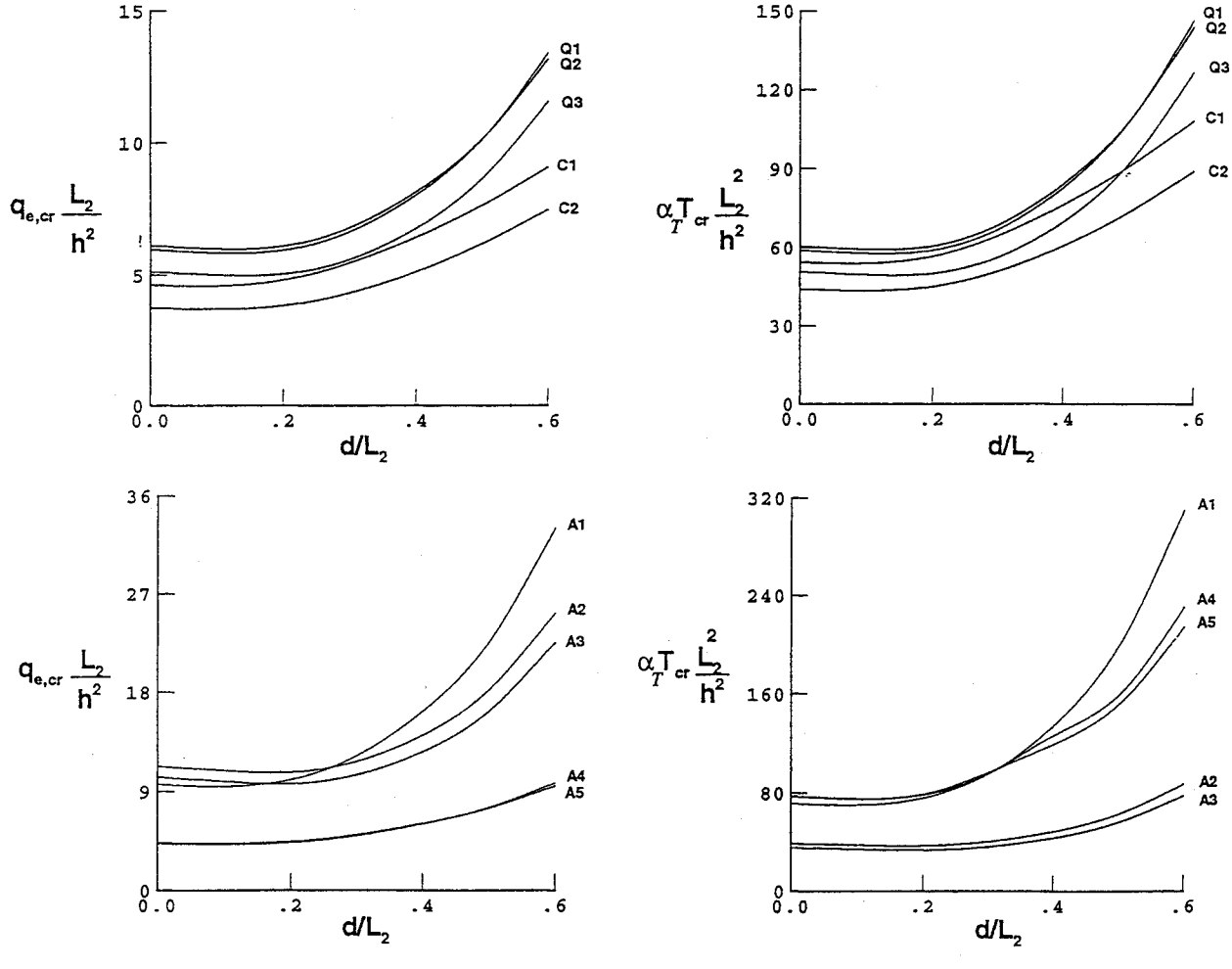

Fig. 2a Effect of hole diameter on the critical values of T_{cr} and $q_{e,cr}$ for 16-layer panels with boundary conditions type 2d; $L_1/L_2 = 1.0$.

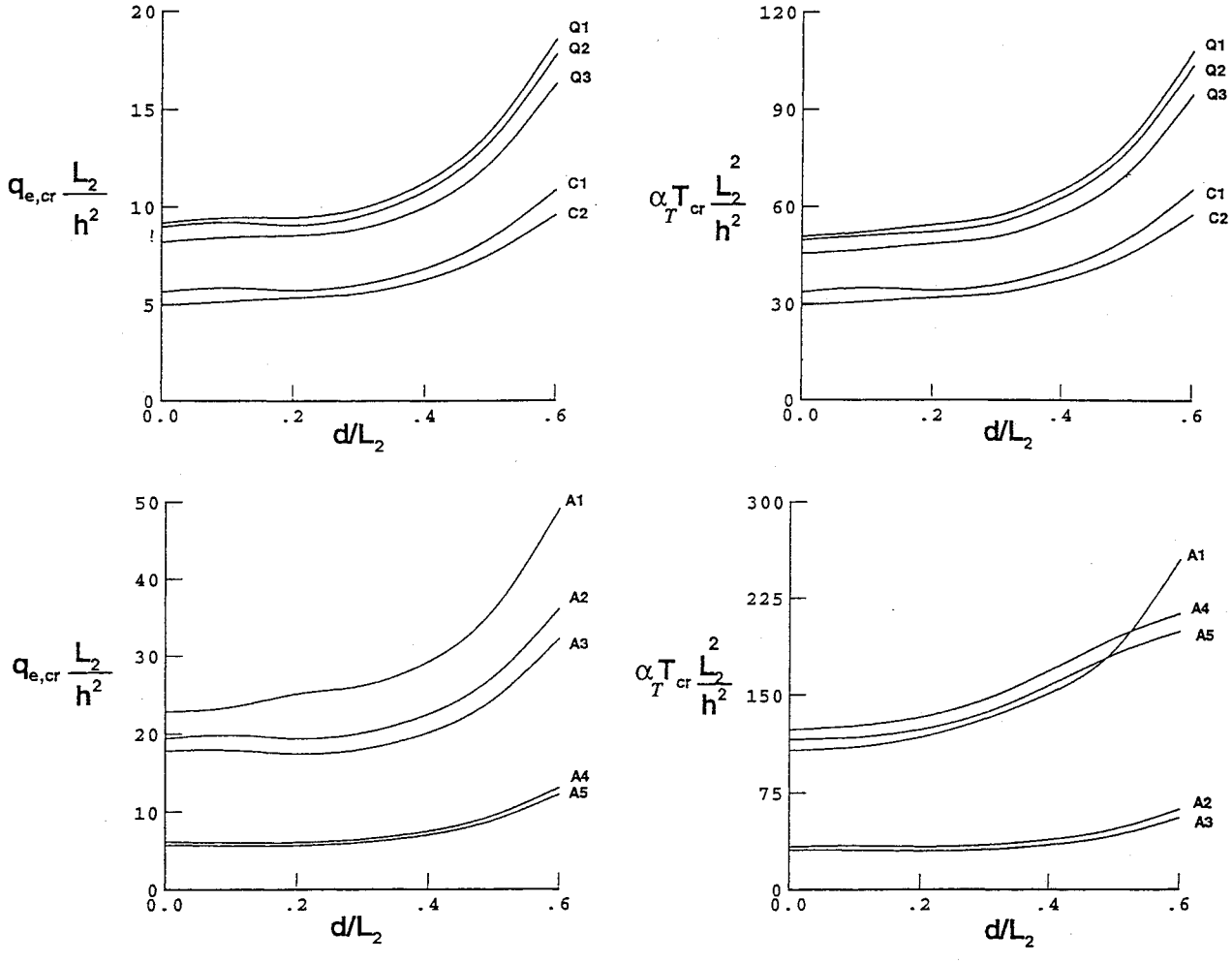

Fig. 2b Effect of hole diameter on the critical values of T_{cr} and $q_{e,cr}$ for 16-layer panels with boundary conditions type 2d; $L_1/L_2 = 2.0$.

modes). The Rayleigh-Ritz technique is then used to approximate the linear algebraic eigenvalue problem by a much smaller eigenvalue problem, with the unknowns being the amplitudes of these modes. An effective set of modes was found to be the path derivatives of the problem (i.e., the various-order derivatives of the response quantities with respect to the load parameters q_1 and q_2). The equations used in evaluating the path derivatives are obtained by successive differentiation of the original nonlinear equations with respect to q_1 and q_2. The left-hand-side matrix in these equations is the same as that of Eq. (2). The details of applying multiple-parameter reduction methods to the determination of the stability boundary are given in Refs. 12 and 13. They involve evaluation of the path derivatives at $q_1 = q_2 = 0$, generation of the reduced eigenvalue problem that approximates the original eigenvalue problem, Eqs. (3), and repeated solution of the reduced eigenvalue problem for different combinations of $\hat{q}_1$ and $\hat{q}_2$.

Numerical Studies

To study the effects of variations in the hole size, laminate stacking sequence, and fiber orientation on the thermomechanical prebuckling and buckling response characteristics and their sensitivity coefficients, several buckling problems of panels were solved. The loading on the panels consisted of a uniform temperature change T_0, an applied edge compressive loading $\bar{N}_1$, and an applied edge displacement q_e. Henceforth, the three separate loading cases will be referred to as the T_0 case, the $\bar{N}_1$ case, and the q_e case, respectively. For each problem, the derivatives of the critical combination of temperature change and the applied edge loading (or edge displacement), with respect to the different material and lamination parameters, were evaluated. The six types of boundary conditions given in Table 1 were considered.

The six types of boundary conditions can be divided into two groups. The first group has the edge displacement u_1 prescribed at $x_1 = \pm L_1/2$, and the second group has the edge loading $\bar{N}_1$ prescribed along those edges. The two groups are identified with the letters d and L, respectively. In all of the boundary condition types the transverse displacement w is restrained along all of the edges, and the in-plane displacement u_2 is restrained at $x_1 = \pm L_1/2$. In addition, for boundary condition types 2 and 3, the rotation ϕ_1 is restrained at $x_1 = \pm L_1/2$, and for boundary condition type 3, the in-plane displacement u_2 is restrained at $x_2 = \pm L_1/2$.

Five parameters were varied, namely, the aspect ratio of the panel, hole diameter, fiber orientation angle, laminate stacking sequence, and number of layers. Cross-ply, quasi-isotropic, and anisotropic panels were considered. The fiber orientation, stacking sequence, and designation of the panels used in the present study are shown in Table 2. The material properties and geometric characteristics of the panel are given in Fig. 1. The material properties, the fiber orientation, and the stacking sequence selected are typical of composite panels considered for future high-performance aircraft. Mixed finite element models were used for the discretization of each panel. Biquadratic shape functions were used for approximating each of the generalized displacements, and bilinear shape functions were used for approximating each of the stress resultants. The characteristics of the finite element model are given in Ref. 14. For each panel, the multiple-parameter reduction methods outlined in Refs. 12 and 13 were used in determining the stability boundary and in evaluating the sensitivity coefficients. Typical results are presented in Figs. 2–10 and are described subsequently.

An examination of the stiffness coefficients of the different panels reveals that the panels with adjacent +45- and −45-deg layers have the same extensional stiffnesses A_{11}, A_{22}, A_{12}, and A_{66} as the

corresponding panels with nonadjacent +45- and –45-deg layers. However, their bending stiffness coefficients D_{12} and D_{66} are higher, and their anisotropic stiffness coefficients D_{16} and D_{26} are lower than those with nonadjacent +45- and –45-deg layers.

For a given number of layers, panel A1 has the highest values of D_{12} and D_{66}, and panels C1, C2 have the lowest values of these coefficients. Panels Q2 and A5 have higher values of D_{11} and lower values of D_{22} than the corresponding panels (Q1, Q3) and A4, respectively.

All of the bifurcation buckling modes of the panels considered exhibit either inversion symmetry or antisymmetry. The inversion symmetry is characterized by the following relations for the generalized displacements:

$$\begin{aligned} w(x_1, x_2) &= w(-x_1, -x_2) \\ \phi_\beta(x_1, x_2) &= -\phi_\beta(-x_1, -x_2) \end{aligned} \tag{6}$$

For the inversion antisymmetry, the right-hand sides of Eqs. (6) are multiplied by a minus sign.

The effects of varying the stacking sequence and the hole diameter on the critical values of T_0 and q_e are shown in Fig. 2 for both square and rectangular panels with $L_1/L_2 = 2$. As can be seen in Fig. 2, for $d/L_2 \geq 0.25$, the critical values of both q_e and T_0 increase as the hole diameter increases. The increase is more pronounced for the quasi-isotropic panels than for the cross-ply panels and for the panel A1 than for the other anisotropic panels. The increase in the critical values with increasing d/L may be attributed to the redistribution of the prebuckling stresses and the associated reduction in N_{11} in a significant area of the panel. The reduction in N_{11} is more noticeable for $d/L \geq 0.3$. The critical values of both q_e and T_0 for the anisotropic panel A1 are higher than those for the corresponding cross-ply and quasi-isotropic panels. Higher critical values of q_e and T_0 are also observed for panels A2 and A3 and for panels A4 and A5, respectively, than for the corresponding cross-ply and quasi-isotropic panels.

The nonmonotonic variation of the critical values with d/L_2 for some of the panels shown in Fig. 2 is due to a mode change that occurs at some values of d/L_2 (the buckling mode changes from a symmetric to an antisymmetric mode or vice versa).

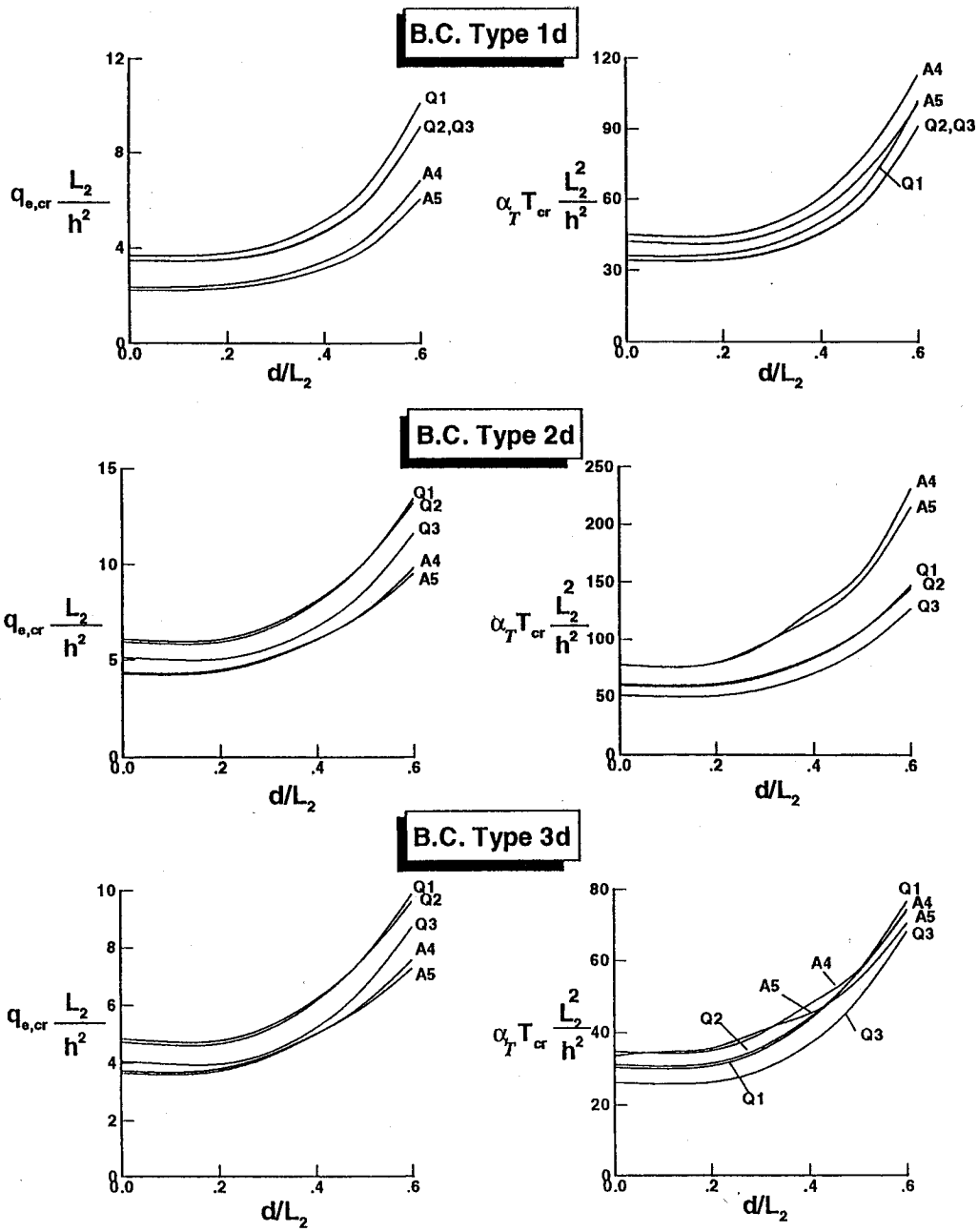

Fig. 3a Effect of boundary conditions on the critical values of T_0 and q_e for panels Q1, Q2, Q3, A4, and A5; $L_1/L_2 = 1.0$; prescribed edge displacement u_1.

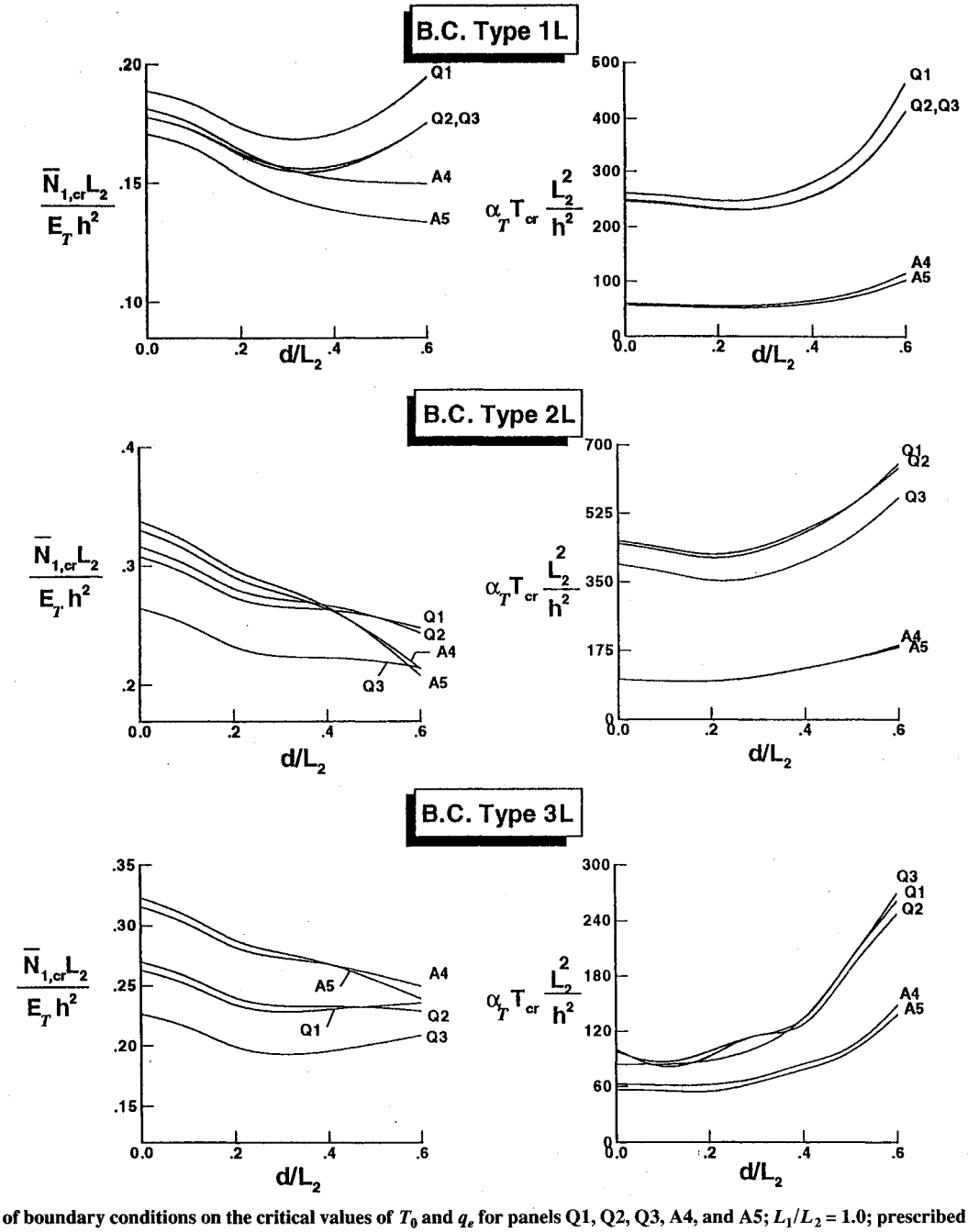

Fig. 3b Effect of boundary conditions on the critical values of T_0 and q_e for panels Q1, Q2, Q3, A4, and A5; $L_1/L_2 = 1.0$; prescribed edge loading $\bar{N}_1$.

Note that, in general, the panels with adjacent +45- and –45-deg layers have higher critical values of q_e and T_0 than the corresponding panels with nonadjacent +45- and –45-deg layers. Exceptions to this are 1) the square panel Q1 with $d/L_2 < 0.5$, for which the critical values of q_e and T_0 are lower than those for the corresponding panel Q2, and 2) the square panel A4 with $d/L_2 < 0.5$, for which the critical value of q_e is lower than that for the corresponding panel A5.

The effect of the boundary conditions on the critical values of q_e, $\bar{N}_1$, and T_0 for the square quasi-isotropic and anisotropic panels is shown in Fig. 3. As is to be expected, the magnitudes of the critical q_e, $\bar{N}_1$, and T_0 and their variations with d/L_2 are strongly affected by the boundary conditions. For all of the panels considered, the critical values of q_e, $\bar{N}_1$, and T_0 decrease when u_2 is restrained at $x_2 = \pm L_2/2$. This result can be seen by comparing the solutions for boundary condition type 3 with the corresponding ones for boundary condition type 2 (see Table 1). The decrease in the critical values may be attributed to the increase in the magnitude of the prebuckling stress resultant N_{22} resulting from restraining u_2. The increase is more pronounced for the T_0 case than for both the q_e and $\bar{N}_1$ cases. However, as for panels with no cutouts, the critical values increase by restraining the rotation ϕ_1 at the edges $x_1 = \pm L_1/2$ (compare solutions for boundary condition 1 with the corresponding solutions for boundary condition 2). As can be seen in Fig. 3, for panels with $d/L_2 \geq 0.3$, the critical values of q_e and T_0 generally increase with increasing d/L_2. This result is true for all of the boundary conditions considered. However, the critical values of $\bar{N}_1$ decrease with increasing d/L_2 for the panels C1, C2, A4, and A5. Also, the critical values of $\bar{N}_1$ decrease with decreasing d/L_2 for the panels Q1, Q2, and Q3 with boundary condition type 2*L*. However, for the same panels Q with $d/L_2 > 0.3$ and with boundary condition types 1*L* and 3*L*, the critical values of $\bar{N}_1$ increase with increasing d/L_2.

When the rotation ϕ_1 is not restrained at the edges $x_1 = \pm L_1/2$ (boundary condition types 1*L* and 1*d*), the panels with adjacent +45- and –45-deg layers have higher critical values of q_e, $\bar{N}_1$, and T_0 than the corresponding panels with nonadjacent +45- and –45-deg layers, regardless of the ratio d/L_2. However, when ϕ_1 is restrained at $x_1 = \pm L_1/2$, higher critical values for panels with adjacent +45- and –45-deg layers are observed only when $d/L_2 > 0.5$.

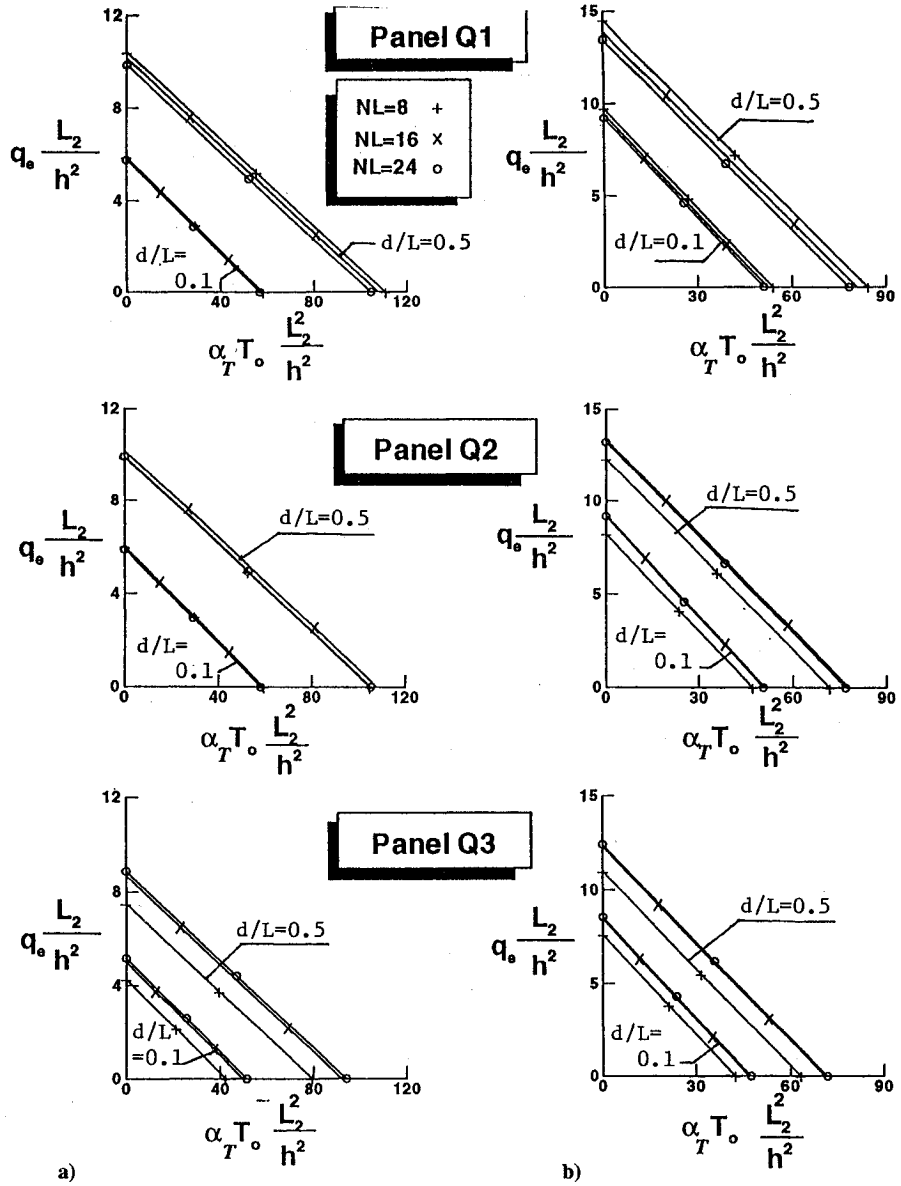

Fig. 4 Effects of number of layers and stacking sequence on the stability boundary for quasi-isotropic panels, $d/L_2 = 0.1$ and 0.5; boundary conditions type 2d: a) $L_1/L_2 = 1.0$ and b) $L_1/L_2 = 2.0$.

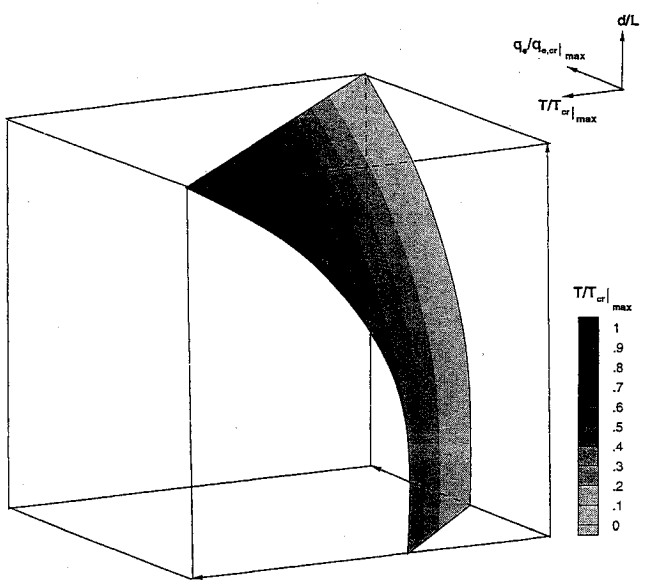

Fig. 5 Surface plot depicting the effect of hole diameter on the stability boundary for 16-layer quasi-isotropic panel Q1, $L_1/L_2 = 1$; boundary conditions type 2d.

The thermomechanical stability boundaries for quasi-isotropic panels Q1, Q2, and Q3 are shown in Fig. 4. Panels with 8, 16, and 24 layers; $d/L_2 = 0.1$ and 0.5; and aspect ratios 1 and 2 are considered. In the figure the applied edge displacement q_e is normalized by the width L_2 and the thickness h, and the temperature change T_0 is normalized by the transverse coefficient of thermal expansion α_T, L_2, and h. Note that when $d/L_2 = 0.5$, panels Q1, with adjacent +45- and −45-deg layers, have higher critical values for q_e and T_0 than the corresponding panels Q2 and Q3 with nonadjacent +45- and −45-deg layers. The differences are more pronounced for the thin eight-layer panels than for the thicker panels. For the panels Q1, the stability boundary moves inward as the number of layers NL increases. An opposite trend is observed for the panels Q3. For square panels Q2, the stability boundaries for the 8-layer and 24-layer panels are almost coincident and move outward as the number of layers changes to 16. When the aspect ratio is 2, for panels Q2 and Q3, the stability boundaries corresponding to $NL = 16$ and 24 are almost coincident. As the number of layers increases beyond 24, the stability boundary becomes insensitive to the relative locations of the +45- and −45-deg layers.

A pictorial surface representation of the effect of the hole diameter ($d/L_2 = 0$–0.6) on the stability boundary for 16-layer panels Q1 is shown in Fig. 5. Figure 5 shows that for a given value of d/L_2 the stability boundary is nearly a straight line. The shading on the surface represents the value of T_0 in the critical combination of T_0 and

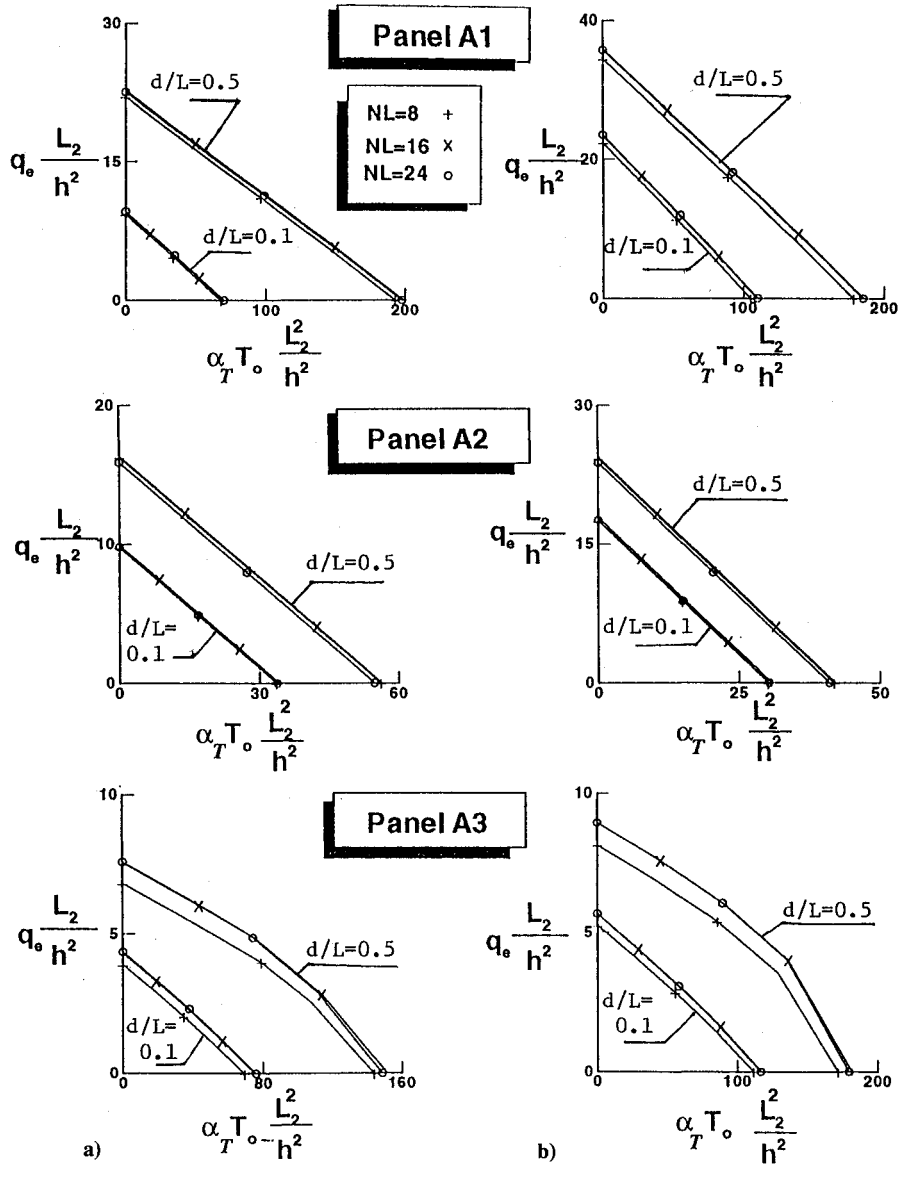

Fig. 6 Effect of number of layers and stacking sequence on the stability boundary for anisotropic panels, $d/L_2 = 0.1$ and 0.5; boundary conditions type 2d: a) $L_1/L_2 = 1.0$ and b) $L_1/L_2 = 2.0$.

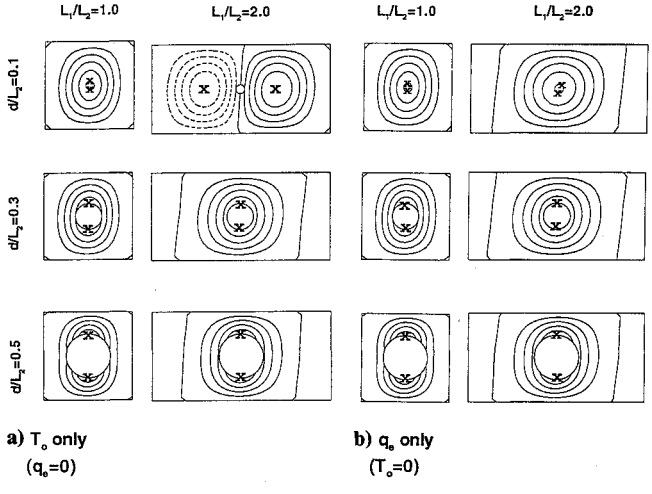

Fig. 7 Effect of hole diameter on the buckling mode shapes associated with the lowest eigenvalues for 16-layer quasi-isotropic panel Q1 with boundary conditions type 2d. Spacing of contour lines is 0.2, and dashed lines denote negative contours. Locations of maximum absolute values are identified with ×: a) $L_1/L_2 = 1.0$ and b) $L_1/L_2 = 2.0$.

q_e, normalized by dividing it by the maximum critical temperature T_{crlmax}.

The stability boundaries for the anisotropic panels A1, A3, and A5 are shown in Fig. 6. Panels with 8, 16, and 24 layers; $d/L_2 = 0.1$ and 0.5; and aspect ratios 1 and 2 are considered. The panels A1, with ±45-deg layers, have higher critical values for T_0 and q_e than the other panels. For a given d/L_2, the stability boundaries for the panels A1 and A3 are straight lines. However, for the panels A5, the stability boundaries are not straight lines because of a mode change (from symmetric to antisymmetric) for $d/L_2 = 0.5$. For panels A1 and A3 the stability boundary moves outward as the number of layers increases above eight. However, the stability boundaries corresponding to $NL = 16$ and 24 are almost coincident.

The effect of increasing the hole diameter on the lowest buckling modes of the 16-layer panels Q1 is shown in Fig. 7. The two cases of $T_0 = 0$ and $q_e = 0$ and the two aspect ratios 1 and 2 are considered. As the hole diameter increases, higher displacement gradients are observed in the vicinity of the cutout. Also, for the T_0 case, panels with aspect ratio of 2 experience a mode change (from antisymmetric to symmetric) when $d/L_2 \geq 0.2$.

The effect of increasing the hole diameter on the lowest buckling mode, associated with the critical temperature for the 16-layer anisotropic panels A1, A3, and A5, is shown in Fig. 8. Panels with aspect ratios 1 and 2 are considered. As for the quasi-isotropic pan-

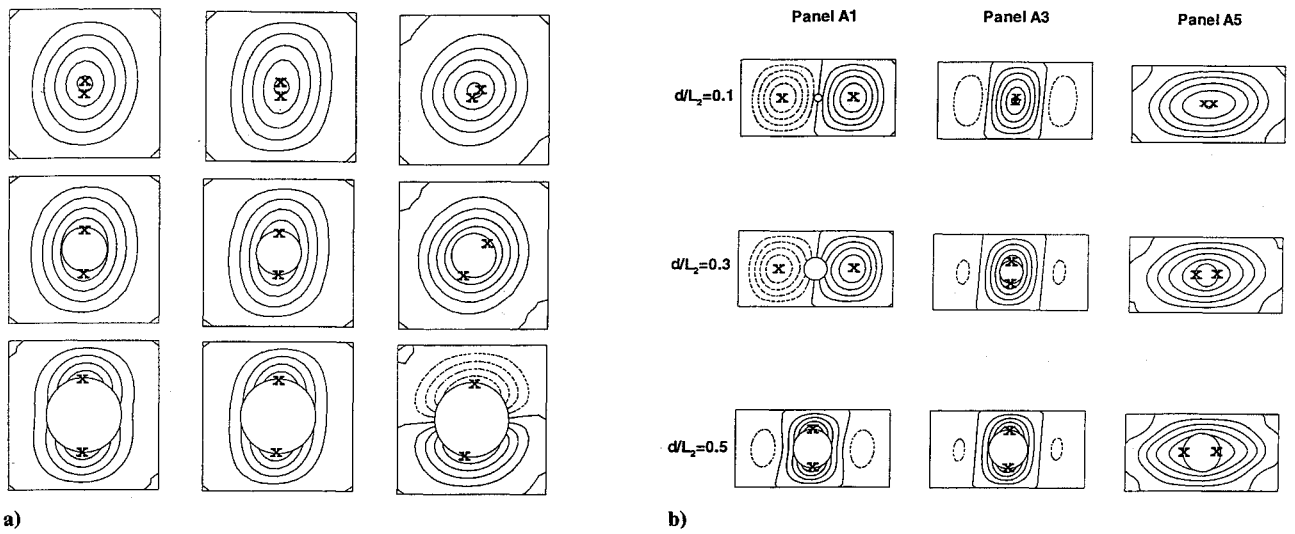

Fig. 8 Effect of hole diameter on the buckling mode shapes associated with the minimum critical temperature T_{cr} for 16-layer anisotropic panels A1, A3, and A5 with boundary conditions type 2d. Spacing of contour lines is 0.2, and dashed lines denote negative contours. Locations of maximum absolute values are identified with ×: a) $L_1/L_2 = 1.0$ and b) $L_1/L_2 = 2.0$.

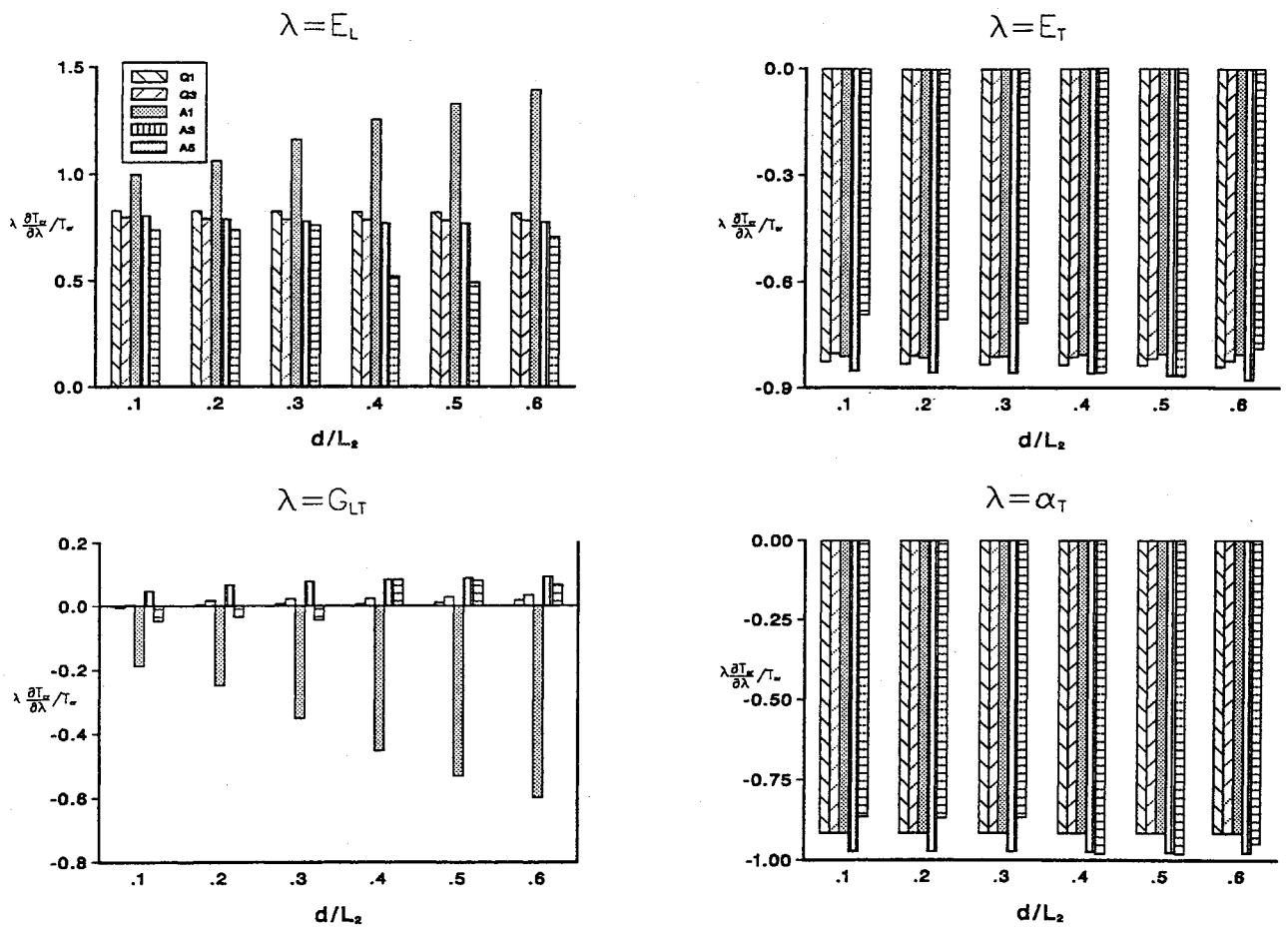

Fig. 9 Sensitivity of the critical temperature T_{cr} to variations in hole diameter and material properties of individual layers. Square 16-layer composite panels with boundary conditions type 2d.

els, higher displacement gradients are developed near the cutout for $d/L_2 \geq 0.3$. Moreover, for $L_1/L_2 = 1$, a mode change (from symmetric to antisymmetric) occurs in panel A5 for $d/L_2 \geq 0.4$, and for $L_1/L_2 = 2$, a mode change (from antisymmetric to symmetric) occurs in panel A1 for $d/L_2 \geq 0.4$.

Sensitivity Studies

Sensitivity analyses were conducted to identify which material parameters most affected the buckling response. The sensitivity of the minimum critical temperature to variations in the four material parameters E_L, E_T, G_{LT}, and α_T and the four fiber angles +45, −45, 0, and 90 deg are shown in Figs. 9 and 10. Both the quasi-isotropic panels Q1 and Q3 and the anisotropic panels A1, A3, and A5 are considered. The effect of the hole size on the normalized sensitivity coefficients $\lambda(\partial T/\partial\lambda)/T_{cr}$, where $\lambda = E_L$, E_T, G_{LT}, and α_T for the five panels is shown in Fig. 9. As can be seen in Fig. 9, most of the sensitivity coefficients do not change much with changes in d/L_2. Exceptions are the case of $\lambda = G_{LT}$ for panels A1, A5, and

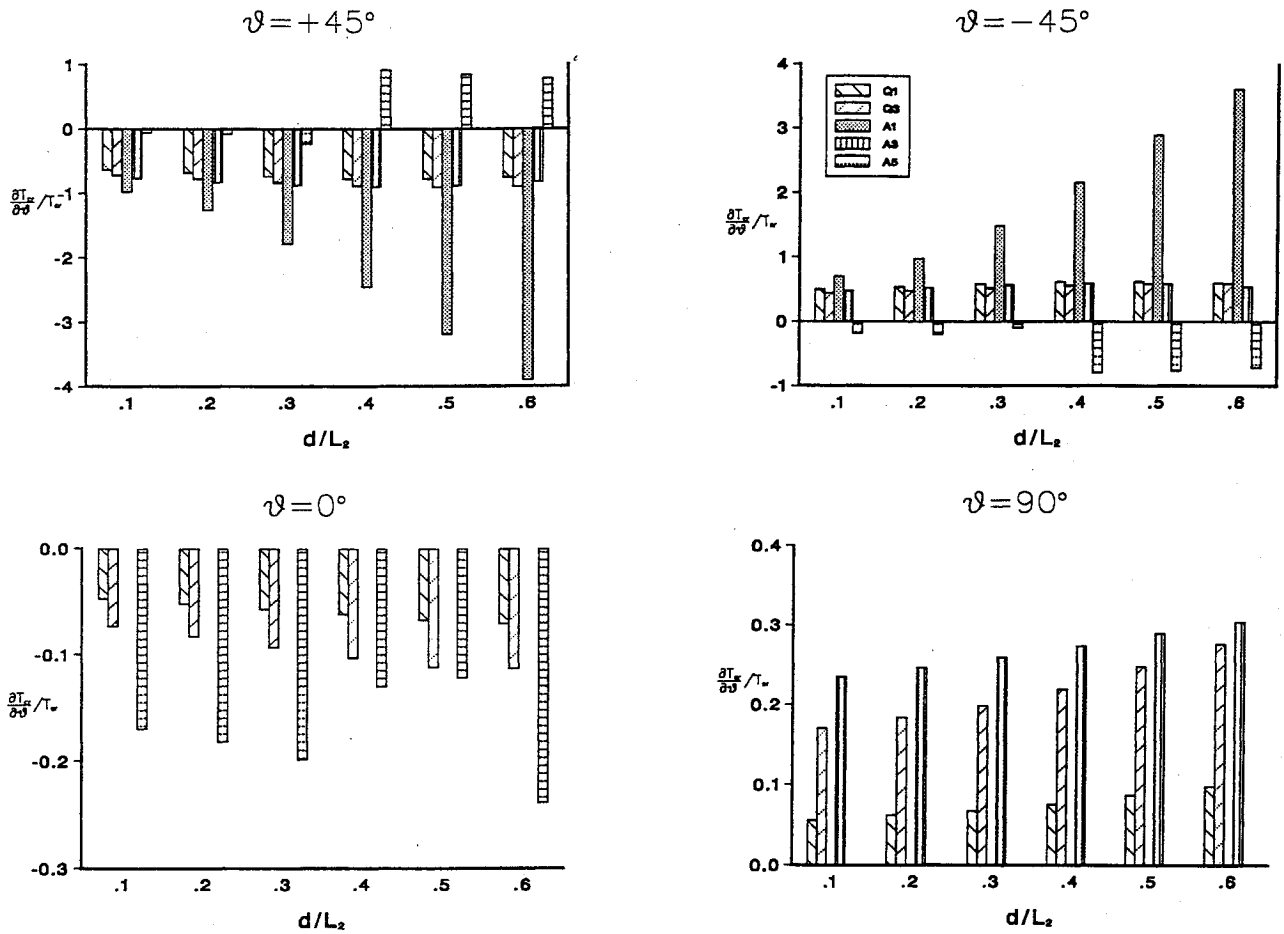

Fig. 10 Sensitivity of the critical temperature T_{cr} to variations in hole diameter and fiber orientation angles of different layers. Square 16-layer composite panels with boundary conditions type 2d.

Q1; the case of $\lambda = E_L$ for panel A1; and the case of $\lambda = \alpha_T$ for panel A5.

The effect of the hole size on the normalized sensitivity coefficients $(\partial T/\partial\theta)/T_{cr}$ is shown in Fig. 10. As can be seen in Fig. 10, d/L_2 has a pronounced effect on $(\partial T/\partial\theta)/T_{cr}$. This observation is particularly true for $\theta = +45$ and -45 deg (panel A1); $\theta = 90$ deg (panel A3); $\theta = +45, -45$, and 0 deg (panel A5); and $\theta = 0$ and 90 deg (panel Q3).

The variation of the sensitivity coefficients with d/L_2 was found to be insensitive to the aspect ratio L_1/L_2.

Concluding Remarks

A study has been made of the buckling response of flat unstiffened composite panels, with central circular holes, subjected to combined temperature change and applied edge loading (or edge displacement). The panels considered consist of a number of perfectly bonded layers and are symmetrically laminated with respect to the middle plane. The analysis is based on a first-order shear deformation plate theory, in which the effects of both laminated anisotropic material behavior and average transverse shear deformation through the thickness are included. A linear, Duhamel-Neumann-type constitutive model is used, and the material properties are assumed to be independent of temperature. The panels have been discretized by using two-field mixed finite element models with the fundamental unknowns consisting of the nodal displacements and stress-resultant parameters. The stress resultants are allowed to be discontinuous at interelement boundaries.

An efficient multiple-parameter reduction method has been used for determining the stability boundary as well as for evaluating the sensitivity coefficients that measure the sensitivity of the buckling response to variations in the different lamination and material parameters of the panel. Numerical results are presented that show the effects of variations in the aspect ratio of the panel, hole diameter, fiber orientation angle, laminate stacking sequence, and number of layers on the thermomechanical buckling response and its sensitivity coefficients.

The lamination parameters (viz., stacking sequence, fiber orientation, and number of layers) can significantly affect the relative stiffnesses of the panel. The numerical results presented show a complex interplay between the relative stiffnesses and the panel, the hole diameter, the aspect ratio, the boundary conditions, and the loading. The effect of the individual parameters on the critical values cannot be easily delineated. However, the following observations and conclusions can be made:

1) As is to be expected, the magnitudes of the critical loads and their variation with the hole diameter are strongly dependent on the boundary conditions and the stacking sequence. The stiffness of the panel and hence the critical values increase by restraining the rotation of the loaded edge and decrease by restraining the in-plane displacement normal to the unloaded edge. The latter may be attributed to the increase in the prebuckling stress resultant N_{22}, particularly for the case of temperature change.

2) In general, for panels with $d/L_2 > 0.3$, the critical loads increase as the hole diameter increases. Exceptions to this result are the critical compressive loads for cross-ply panels, anisotropic panels with combinations of ±45- and 90-deg layers, and the quasi-isotropic panels with both the rotations of the loaded edges restrained and the in-plane displacements of the unloaded edges unrestrained. The increase in the critical values with increasing d/L_2 may be attributed to the redistribution of the prebuckling stresses and the associated reduction in N_{11} in a significant area of the panel.

3) When the edge rotation is not restrained, the panels with adjacent +45- and −45-deg layers have higher values for the critical loads and critical temperatures than the corresponding panels with

nonadjacent +45- and −45-deg layers. This result is true for all of the hole diameters considered in the present study. On the other hand, when the edge rotation is restrained, higher critical values for panels with adjacent +45- and −45-deg layers are observed only for large hole diameters, $d/L_2 > 0.5$.

4) For a given hole diameter, the thermomechanical interaction curve (stability boundary) is a straight line. Exceptions to this result are cases for which a mode change occurs (from symmetric to antisymmetric mode or vice versa) at a particular combination of thermal and mechanical loads.

5) The normalized sensitivity coefficients of the critical temperature for quasi-isotropic and anisotropic panels with combinations of +45-, −45-, and 0-deg layers do not change much with changing the hole diameter. However, some of the sensitivity coefficients for anisotropic panels with no 0-deg layers, change significantly with the change in the hole diameter.

Appendix A: Thermoelastic Constitutive Relations for the Laminate

The thermoelastic model used in the present study is based on the following assumptions.

1) The laminates are composed of a number of perfectly bonded layers.

2) Every point of the laminate is assumed to possess a single plane of thermoelastic symmetry parallel to the middle plane.

3) The material properties are independent of temperature.

4) The constitutive relations are described by the lamination theory and can be written in the following compact form:

$$\begin{Bmatrix} N \\ M \\ Q \end{Bmatrix} = \begin{bmatrix} [A] & [B] & 0 \\ [B]^t & [D] & 0 \\ 0 & 0 & [A_s] \end{bmatrix} \begin{Bmatrix} \varepsilon \\ \kappa \\ \gamma \end{Bmatrix} - \begin{Bmatrix} N_T \\ M_T \\ 0 \end{Bmatrix} \tag{A1}$$

where $\{N\}$, $\{M\}$, $\{Q\}$, $\{\varepsilon\}$, $\{\kappa\}$, and $\{\gamma\}$ are given by

$$\{N\}^t = [N_1 \quad N_2 \quad N_{12}] \tag{A2}$$

$$\{M\}^t = [M_1 \quad M_2 \quad M_{12}] \tag{A3}$$

$$\{Q\}^t = [Q_1 \quad Q_2] \tag{A4}$$

$$\{\varepsilon\}^t = [\varepsilon_1 \quad \varepsilon_2 \quad 2\varepsilon_{12}] \tag{A5}$$

$$\{\kappa\}^t = [\kappa_1 \quad \kappa_2 \quad 2\kappa_{12}] \tag{A6}$$

$$\{\gamma\}^t = [2\varepsilon_{13} \quad 2\varepsilon_{23}] \tag{A7}$$

The matrices $[A]$, $[B]$, $[D]$, and $[A_s]$ can be expressed in terms of the layer stiffnesses as follows:

$$[[A]\,[B]\,[D]] = \sum_{k=1}^{NL} \int_{h_{k-1}}^{h_k} [\bar{Q}]^{(k)} \,[[I] \quad x_3[I] \quad (x_3)^2[I]]\, dx_3 \tag{A8}$$

$$[A_s] = \sum_{k=1}^{NL} \int_{h_{k-1}}^{h_k} [\bar{Q}_s]^{(k)}\, dx_3 \tag{A9}$$

where $[I]$ is the identity matrix and h_k and h_{k-1} are the distances from the top and bottom surfaces of the kth layer to the middle surface. The expressions for the different coefficients of the matrices $[\bar{Q}]^{(k)}$ and $[\bar{Q}_s]^{(k)}$ in terms of the material and geometric properties of the constituents (fiber and matrix) are given in Refs. 15 and 16.

The vectors of thermal forces and moments $\{N_T\}$ and $\{M_T\}$ are given by

$$[\{N_T\}\ \{M_T\}] = \sum_{k=1}^{NL} \int_{h_{k-1}}^{h_k} [\bar{Q}]^{(k)} \{\alpha\}^{(k)} [1 \quad x_3] T\, dx_3 \tag{A10}$$

(See, for example, Refs. 17 and 18.)

Appendix B: Form of the Arrays in the Governing Discrete Equations of the Panel

The governing discrete equations of the panel, Eqs. (1), consist of both the constitutive relations and the equilibrium equations. The response vector $\{Z\}$ can be partitioned into the subvectors of stress-resultant parameters $\{H\}$ and the free (unconstrained) nodal displacements $\{X\}$ as follows:

$$\{Z\} = \begin{Bmatrix} H \\ X \end{Bmatrix} \tag{B1}$$

The different arrays in Eqs. (1–4) can be partitioned as follows:

$$[\bar{K}] = \begin{bmatrix} -F & S_1 \\ S_1^t & 0 \end{bmatrix} \tag{B2}$$

$$\{\bar{G}(Z)\} = \begin{Bmatrix} \bar{M}(X, \bar{X}_e) \\ \bar{N}(H, X, \bar{X}_e) \end{Bmatrix} \tag{B3}$$

$$\{\bar{Q}^{(1)}\} = \begin{Bmatrix} \varepsilon_T \\ 0 \end{Bmatrix} \tag{B4}$$

$$\{\bar{Q}^{(2)}\} = \begin{Bmatrix} 0 \\ P \end{Bmatrix} \tag{B5}$$

for the applied edge loading case and

$$\{\bar{Q}^{(2)}\} = \begin{Bmatrix} -[S_2]\,\{\bar{X}_e\} \\ 0 \end{Bmatrix} \tag{B6}$$

for the applied edge displacement case and

$$[\bar{K}_1] = \begin{bmatrix} 0 & 0 \\ 0 & [K_1] \end{bmatrix} \tag{B7}$$

$$[\bar{K}_2] = \begin{bmatrix} 0 & 0 \\ 0 & [K_2] \end{bmatrix} \tag{B8}$$

$$\left[\frac{\partial \bar{K}}{\partial \lambda_\ell}\right] = \begin{bmatrix} -\left[\frac{\partial F}{\partial \lambda_\ell}\right] & 0 \\ 0 & 0 \end{bmatrix} \tag{B9}$$

$$\left\{\frac{\partial \bar{Q}^{(1)}}{\partial \lambda_\ell}\right\} = \begin{Bmatrix} \frac{\partial \varepsilon_T}{\partial \lambda_\ell} \\ 0 \end{Bmatrix} \tag{B10}$$

where 0 refers to a null matrix or vector. For the case of applied edge forces, $\{\bar{X}_e\}$ in Eqs. (B3) is absent.

For the purpose of obtaining analytic derivatives with respect to lamination parameters (e.g., fiber orientation angle of different

layers), it is convenient to express $(\partial[F]/\partial\lambda_\ell)$ in terms of $(\partial[F]^{-1}/\partial\lambda_\ell)$ as follows:

$$\frac{\partial[F]}{\partial\lambda_\ell} = -[F]\frac{\partial[F]^{-1}}{\partial\lambda_\ell}[F] \tag{B11}$$

The explicit forms of $(\partial[F]^{-1}/\partial\lambda_\ell)$ and $\{\partial\varepsilon_T/\partial\lambda_\ell\}$ are given in Appendix C.

Appendix C: Explicit Forms of λ_ℓ

It is convenient to partition the matrices $[F]^{-1}$ and $(\partial[F]^{-1}/\partial\lambda_\ell)$ for individual elements, into blocks and to partition the vectors $\{\varepsilon_T\}$ and $\partial\{\varepsilon_T\}/\partial\lambda_\ell$ into subvectors.

The expression of a typical block (i', j') of $\partial[F]^{-1}/\partial\lambda_\ell$ is given by

$$\frac{\partial}{\partial\lambda_\ell}[F]^{-1}_{i',j'} = \int_{\Omega^{(e)}} N_{i'}N_{j'}\frac{\partial}{\partial\lambda_\ell}\begin{bmatrix}[A] & [B] & 0\\ [B]^t & [D] & 0\\ 0 & 0 & [A_s]\end{bmatrix} d\Omega \tag{C1}$$

where

$$\frac{\partial}{\partial\lambda_\ell}\begin{Bmatrix}[A]\\ [B]\\ [D]\end{Bmatrix} = \sum_{k=1}^{NL}\int_{h_{k-1}}^{h_k}\frac{\partial}{\partial\lambda_\ell}[\bar{Q}]^{(k)}\begin{Bmatrix}1\\ x_3\\ (x_3)^2\end{Bmatrix} dx_3 \tag{C2}$$

$$\frac{\partial}{\partial\lambda_\ell}[A_s] = \sum_{k=1}^{NL}\int_{h_{k-1}}^{h_k}\frac{\partial}{\partial\lambda_\ell}[\bar{Q}_s]^{(k)}\, dx_3 \tag{C3}$$

where $\Omega^{(e)}$ is the element domain.

The expression of a typical partition i' of the thermal strain vector $\{\varepsilon_T\}$ is given by

$$\{\varepsilon_T\}_{i'} = \int_{\Omega^{(e)}}\begin{bmatrix}[A] & [B] & 0\\ [B]^t & [D] & 0\\ 0 & 0 & [A_s]\end{bmatrix}^{-1}\begin{Bmatrix}N_T\\ M_T\\ 0\end{Bmatrix}N_{i'}\, d\Omega \tag{C4}$$

The expression of a typical partition i' of the vector $\{\partial\varepsilon_T/\partial\lambda_\ell\}_{i'}$ is given by

$$\begin{Bmatrix}\partial\varepsilon_T\\ \overline{\partial\lambda_\ell}\end{Bmatrix}_{i'} = \int_{\Omega^{(e)}}\left(\frac{\partial}{\partial\lambda_\ell}\begin{bmatrix}[A] & [B] & 0\\ [B]^t & [D] & 0\\ 0 & 0 & [A_s]\end{bmatrix}^{-1}\begin{Bmatrix}N_T\\ M_T\\ 0\end{Bmatrix}\right.$$

$$\left. + \begin{bmatrix}[A] & [B] & 0\\ [B]^t & [D] & 0\\ 0 & 0 & [A_s]\end{bmatrix}^{-1}\frac{\partial}{\partial\lambda_\ell}\begin{Bmatrix}N_T\\ M_T\\ 0\end{Bmatrix}\right)N_{i'}\, d\Omega \tag{C5}$$

where

$$\frac{\partial}{\partial\lambda_\ell}\begin{bmatrix}[A] & [B] & 0\\ [B]^t & [D] & 0\\ 0 & 0 & [A_s]\end{bmatrix}^{-1}$$

$$= -\begin{bmatrix}[A] & [B] & 0\\ [B]^t & [D] & 0\\ 0 & 0 & [A_s]\end{bmatrix}^{-1}\frac{\partial}{\partial\lambda_\ell}\begin{bmatrix}[A] & [B] & 0\\ [B]^t & [D] & 0\\ 0 & 0 & [A_s]\end{bmatrix}$$

$$\times\begin{bmatrix}[A] & [B] & 0\\ [B]^t & [D] & 0\\ 0 & 0 & [A_s]\end{bmatrix}^{-1} \tag{C6}$$

and

$$\frac{\partial}{\partial\lambda_\ell}\Big[\{N_T\}\ \{M_T\}\Big] = \sum_{k=1}^{NL}\int_{h_{k-1}}^{h_k}\left(\frac{\partial[\bar{Q}]^{(k)}}{\partial\lambda_\ell}\{\alpha\}^{(k)}\right.$$

$$\left. + [\bar{Q}]^{(k)}\left\{\frac{\partial\alpha}{\partial\lambda_\ell}\right\}^{(k)}\right)\Big[1\ x_3\Big]T\, dx_3 \tag{C7}$$

Analytic expressions are given in Ref. 19 for the laminate stiffnesses $[A], [B], [D]$, and $[A_s]$; the vectors of thermal effects $\{N_T\}$ and $\{M_T\}$; and their derivatives with respect to each of the material properties and fiber orientation angles.

Acknowledgment

The work of the first and third authors was particularly supported by NASA Cooperative Agreement NCCW-0011 and by NASA Grant NAG-1-1162. The material properties were supplied by the Aircraft Division of Northrop Corporation. The numerical studies were performed on the Cray Y-MP computer at NASA Ames Research Center.

References

[1]Nemeth, M. P., Stein, M., and Johnson, E. R., "An Approximate Buckling Analysis for Rectangular Orthotropic Plates with Centrally Located Cutouts," NASA TP-2528, Feb. 1986.

[2]Nemeth, M. P., "A Buckling Analysis for Rectangular Orthotropic Plates with Centrally Located Cutouts," NASA TM-86263, Dec. 1984.

[3]Nemeth, M. P., "Buckling Behavior of Compression-Loaded Symmetrically Laminated Angle-Ply Plates with Holes," *AIAA Journal*, Vol. 26, No. 3, 1988, pp. 330–336.

[4]Nemeth, M. P., "Buckling and Postbuckling Behavior of Square Compression-Loaded Graphite-Epoxy Plates with Circular Cutouts," NASA TP-3007, Aug. 1990.

[5]Chang, J. S., and Shiao, F. J., "Thermal Buckling Analysis of Isotropic and Composite Plates with a Hole," *Journal of Thermal Stresses*, Vol. 13, No. 3, 1990, pp. 315–332.

[6]Owen, V., and Klang, E. C., "Shear Buckling of Specially Orthotropic Plates with Centrally Located Cutouts," Eighth DOD/NASA/FAA Conf. on Fibrous Composites in Structural Design (Norfolk, VA); NASA CP-3087-PT-2, 1989.

[7]Chen, W. J., Lin, P. D., and Chen, L. W., "Thermal Buckling Behavior of Composite Laminated Plates with a Circular Hole," *Computers and Structures*, Vol. 18, No. 4, 1991, pp. 379–397.

[8]Srivatsa, K. S., and Krishna Murty, A. V., "Stability of Laminated Composite Plates with Cutouts," *Computers and Structures*, Vol. 43, No. 2, 1992, pp. 273–279.

[9]Jones, K. M., and Klang, E. C., "Buckling Analysis of Fully Anisotropic Plates Containing Cutouts and Elastically Restrained Edges," *Proceedings of the AIAA/ASME/ASCE/AHS/ASC 33rd Structures, Structural Dynamics, and Materials Conference* (Dallas, TX), Pt. 1, Structures I, AIAA, Washington, DC, 1992, pp. 190–200.

[10]Lee, H. H., and Hyer, M. W., "Postbuckling Failure of Composite Plates with Holes," *Proceedings of the AIAA/ASME/ASCE/AHS/ASC 33rd Structures, Structural Dynamics, and Materials Conference* (Dallas, TX), Pt. 1, Structures I, AIAA, Washington, DC, 1992, pp. 201–211.

[11]Noor, A. K., Starnes, J. H., Jr., and Peters, J. M., "Thermomechanical Buckling and Postbuckling of Multilayerd Composite Panels," *Composite Structures*, Vol. 23, No. 3, 1993, pp. 233–251.

[12]Noor, A. K., and Peters, J. M., "Multiple-Parameter Reduced Basis Technique for Bifurcation and Postbuckling Analyses of Composite

Plates," *International Journal for Numerical Methods in Engineering*, Vol. 19, No. 12, 1983, pp. 1783–1803.

[13]Noor, A. K., and Peters, J. M., "Recent Advances in Reduction Methods for Instability Analysis of Structures," *Computers and Structures*, Vol. 16, No. 1–4, 1983, pp. 67–80.

[14]Noor, A. K., and Andersen, C. M., "Mixed Models and Reduced/Selective Integration Displacement Models for Nonlinear Shell Analysis," *International Journal for Numerical Methods in Engineering*, Vol. 18, No. 10, 1982, pp. 1429–1454.

[15]Jones, R. M., *Mechanics of Composite Materials*, McGraw-Hill, New York, 1975.

[16]Tsai, S. W., and Hahn, H. T., *Introduction to Composite Materials*, Technomic Publishing, Westport, CT, 1980.

[17]Padovan, J., "Anisotropic Thermal Stress Analysis," *Thermal Stresses I*, edited by R. B. Hetnarski, Mechanics and Mathematical Methods (2nd series), Elsevier, Amsterdam, The Netherlands, 1986, pp. 143–262.

[18]Bert, C. W., "Analysis of Plates," *Structural Design and Analysis, I*, edited by C. C. Chamis, Vol. 7, Composite Materials, Academic, New York, 1975, pp. 149–206.

[19]Noor, A. K., and Tenek, L. H., "Stiffness and Thermal Coefficients for Composite Laminates," *Composite Structures*, Vol. 21, No. 1, 1992, pp. 57–66.